PNAS RESEARCH ARTICLE | BIOCHEMISTRY

In silico identification of a β_2-adrenoceptor allosteric site that selectively augments canonical β_2AR-Gs signaling and function

Sushrut D. Shah[a,1], Christoffer Lind[b,1], Francesco De Pascali[c], Raymond B. Penn[a], Alexander D. MacKerell Jr.[b,2], and Deepak A. Deshpande[a,2]

Edited by Mark Nelson, University of Vermont, Burlington, Vermont; received August 22, 2022; accepted October 26, 2022

Activation of β_2-adrenoceptors (β_2ARs) causes airway smooth muscle (ASM) relaxation and bronchodilation, and β_2AR agonists (β-agonists) are front-line treatments for asthma and other obstructive lung diseases. However, the therapeutic efficacy of β-agonists is limited by agonist-induced β_2AR desensitization and noncanonical β_2AR signaling involving β-arrestin that is shown to promote asthma pathophysiology. Accordingly, we undertook the identification of an allosteric site on β_2AR that could modulate the activity of β-agonists to overcome these limitations. We employed the site identification by ligand competitive saturation (SILCS) computational method to comprehensively map the entire 3D structure of in silico-generated β_2AR intermediate conformations and identified a putative allosteric binding site. Subsequent database screening using SILCS identified drug-like molecules with the potential to bind to the site. Experimental assays in HEK293 cells (expressing recombinant wild-type human β_2AR) and human ASM cells (expressing endogenous β_2AR) identified positive and negative allosteric modulators (PAMs and NAMs) of β_2AR as assessed by regulation of β-agonist-stimulation of cyclic AMP generation. PAMs/NAMs had no effect on β-agonist-induced recruitment of β-arrestin to β_2AR- or β-agonist-induced loss of cell surface expression in HEK293 cells expressing β_2AR. Mutagenesis analysis of β_2AR confirmed the SILCS identified site based on mutants of amino acids R131, Y219, and F282. Finally, functional studies revealed augmentation of β-agonist-induced relaxation of contracted human ASM cells and bronchodilation of contracted airways. These findings identify a allosteric binding site on the β_2AR, whose activation selectively augments β-agonist-induced Gs signaling, and increases relaxation of ASM cells, the principal therapeutic effect of β-agonists.

adrenergic receptor | allosteric modulator | biased signaling | SILCS | asthma

Obstructive lung diseases such as asthma and chronic obstructive pulmonary disease are characterized by increased bronchoconstriction and difficulty in breathing (1). Augmented airway smooth muscle (ASM) contraction contributes significantly to the narrowing of the airway lumen and various G protein-coupled receptors (GPCRs) expressed on the cell surface of ASM regulate contraction or relaxation of ASM, and thus airway patency. Activation of β_2-adrenoceptors (β_2AR) on ASM by endogenous (epinephrine and norepinephrine) and exogenous agonists promotes ASM relaxation and bronchodilation. Thus, synthetic agonists of the β_2AR (β-agonists) have been the principal therapeutic means of relief of acute bronchoconstriction for decades. However, chronic β-agonist use has multiple deleterious effects, including worsening asthma control associated with increased airway hyperresponsiveness and a loss of bronchoprotective effect as well as increased mucus production and indices of airway inflammation (2–5). Of particular note, the findings from the Salmeterol Multi-center Asthma Research Trial (SMART) study raised mortality concerns that ultimately led to a black box warning for long-acting β-agonists and more stringent guidelines for their clinical use (6). These studies underscore the need for drug development strategies for β_2AR ligands/modulators to effectively promote beneficial therapeutic effects while minimizing the deleterious effects of β-agonists.

β-agonists bind to β_2AR at the orthosteric site of the receptor and promote the interaction of the β_2AR with multiple signaling protein assemblies, including those of Gs-protein, G protein receptor kinases, and β-arrestins (7). These signaling proteins are capable of promoting multiple downstream signaling pathways resulting in ASM relaxation, negative feedback regulation (desensitization, receptor internalization), gene expression, and regulation of cell proliferation (8). Numerous cell, tissue, and in vivo studies have attributed the therapeutic effects of β-agonists in asthma to canonical Gs signaling by the β_2AR, while the regulatory effects of β-arrestins constrain such therapeutic efficacy (9–12) by promoting ASM β_2AR desensitization, and reducing canonical Gs-cAMP-PKA signaling and the prorelaxant effect of β-agonists on ASM (9, 12). More recent studies have implicated β-arrestins in β-agonist-induced proinflammatory and pathogenic effects in murine models of asthma (11, 13–18).

Significance

β_2ARs are the primary targets for relieving bronchoconstriction in airway diseases such as asthma and COPD. Activation of airway smooth muscle (ASM) β_2ARs promotes therapeutic effects (via β_2AR-Gs pathway) that are constrained by β_2AR engagement with the regulatory protein β-arrestin. Moreover, chronic activation of β_2AR promotes agonist-specific desensitization that contributes to a loss of β_2AR function and the diminished effectiveness of β-agonists in managing asthma. Using computational approaches, we identified an allosteric site on an intermediate conformation of β_2AR and associated positive modulators that augmented: 1) beneficial signaling mediated via the canonical β_2AR-Gs pathway; 2) relaxation of ASM cells; and 3) dilation of airways ex vivo induced by β-agonists, outcomes that promote therapeutic effects of β-agonists in obstructive lung diseases.

Author contributions: S.D.S., C.L., R.B.P., A.D.M., and D.A.D. designed research; S.D.S., C.L., and F.D.P. performed research; S.D.S., C.L., F.D.P., R.B.P., A.D.M., and D.A.D. analyzed data; A.D.M. obtained funds; D.A.D. secured funding for the research; and S.D.S., C.L., F.D.P., R.B.P., A.D.M., and D.A.D. wrote the paper.

Competing interest statement: The authors have organizational affiliations to disclose; A.D.M. is the co-founder and CSO of SilcsBio LLC. The authors have patent filings to disclose; a provisional patent application has been filed.

This article is a PNAS Direct Submission.

[1]S.D.S. and C.L. contributed equally to this work.

[2]To whom correspondence may be addressed. Email: alex@outerbanks.umaryland.edu or deepak.deshpande@jefferson.edu.

This article contains supporting information online at https://www.pnas.org/lookup/suppl/doi:10.1073/pnas.2214024119/-/DCSupplemental.

Published November 30, 2022.

Development of allosteric modulators of the β_2AR, particularly those capable of augmenting and biasing β_2AR downstream signaling toward (therapeutic) signaling capabilities may overcome the limitations of those β-agonists currently used to manage asthma. Allosteric modulators bind to a receptor at sites distinct from those bound by orthosteric ligands, to either augment (positive allosteric modulator (PAM)) or reduce (negative allosteric modulator (NAM)) the signaling transduced by the orthosteric ligand. Allosteric modulators (AMs) of GPCRs have potential advantages over orthosteric ligands as therapeutic drugs. In the absence of an orthosteric ligand, they lack activity and thus are able to maintain activity dependence of physiological GPCR signaling (19, 20). Moreover, allosteric modulators offer the potential of greater specificity of targeting, given the greater sequence diversity of allosteric modulator binding sites relative to those typically engaged by orthosteric ligands (19, 20). To date, a few allosteric modulators of β_2AR have been identified, with their effects on modulating signaling and arrestin recruitment characterized in HEK293 cells expressing recombinant β_2AR (21–23). Experimental screening using DNA-encoded libraries identified a β_2AR NAM (21, 24) and a PAM (Cmpd 6) (22), with both compounds having similar (negative and positive) modulation of β-agonist-induced cAMP generation and arrestin recruitment. Liu et al. identified a weak β_2AR NAM using in silico docking, and chemical optimization resulted in a balanced NAM for both Gs activation and arrestin recruitment (22). Recent studies report PAM Cmpd 6 acts as a positive modulator of the beta blocker carvedilol, through enhanced binding affinity of carvedilol to β_2AR and enhanced β-arrestin binding (25). Cmpd 6 can also increase the activity of carvedilol (but not of β_1AR agonists) at the β_1AR and β_1AR-arrestin-mediated signaling to confer cardioprotection (26).

In the present study to rationally identify additional allosteric binding sites and small molecules capable of modulating signaling by β_2AR, we applied the site identification by ligand competitive saturation (SILCS) approach (27, 28) using the program Climber (29). The objective of this study was to target an intermediate confirmation between the inactive and the ligand-bound active state of β_2AR. SILCS is a cosolvent molecular simulation approach that maps the functional group affinity pattern of a protein, including the protein interior, taking into account protein flexibility as well as protein and functional group desolvation contributions. Notably, the SILCS-Hotspots method allows for docking a collection of fragments on the entire protein to identify putative binding sites suitable for drug-like molecules (30). The SILCS approach has previously been used to identify allosteric sites on the proteins heme oxygenase (31) and β-Glucosidase A (32). In addition, the SILCS-Pharmacophore (33) and Monte Carlo (SILCS-MC) (34) methods are of utility for identifying drug-like molecules that bind to the targeted sites, an approach we have previously used to identify novel agonists of the β_2AR (35). Accordingly, in the present study, we apply the SILCS toolbox and molecular dynamics (MD) simulations, to identify a previously unidentified allosteric site on β_2AR along with putative AMs that interact with the identified site, which were then subjected to robust signaling and functional characterization. A detailed description of the computational methods is given in the *SI Appendix*.

Signaling studies of the SILCS-selected compounds identified five positive (PAM) and three negative (NAM) allosteric modulators (AMs) of the β_2AR based on their capacity to modulate isoproterenol (ISO)-induced cAMP generation. Interestingly, none of the AMs affected either ISO-induced β-arrestin recruitment to the β_2AR or β_2AR internalization. Computational and mutagenesis studies revealed the requirement of the β_2AR amino acids R131, Y219, and F282 for binding of the AMs. In addition, the positive and negative allosteric modulators (PAMs and NAMs) identified were able to modulate ISO-mediated relaxation of human ASM cells and bronchodilation of airways in human and murine precision-cut lung slices. This work describes the identification of an allosteric site on the β_2AR and characterization of β_2AR AMs that bind to that site capable of selectively enhancing canonical Gs signaling induced by β-agonists in human ASM cells to improve the therapeutic function of the β_2AR. Moreover, this study provides a strategy for discovering AMs of β_2AR that could be applied to other GPCRs with therapeutic promise.

Results

Molecular Dynamics Simulations to Identify Intermediate Conformational States. Molecular modeling and dynamics were applied to identify conformations of the β_2AR intermediate to those of the active and inactive forms of the receptor. This was performed using the protein structure morphing program Climber which identifies conformations between two input conformations (29). Starting from the active conformation, the structure was gradually morphed leading to a decrease in the Climber energy and the root-mean square difference (RMSD) with respect to the inactive conformation. The RMSD increased with respect to the active form (Fig. 1*A*). At the global minimum of the Climber energy, reached at approximately morphing step 160, the receptor attains the inactive conformation with respect to the transmembrane (TM) helices with the subsequent increase in Climber energy associated with the final morphing of loops and side chain atoms. Two conformations, steps 74 and 143, corresponding to energy minima along the morphing trajectory with conformations intermediate to the active and inactive were selected (Fig. 1*A*).

These two conformations were then subjected to a series of MD simulations to comprehensively sample conformational space of the receptor. The simulations were performed on the apo, agonist-bound, and inverse agonist-bound forms of both intermediates, with three individual simulations of each form performed for each of the two intermediates. The ionic-lock distance between residues R131 and E268 was used to define intermediate conformations with respect to the known inactive and active structures. However, if the ionic-lock formed any salt bridge interactions during the simulations, those simulations were not considered further.

Analysis of the sampling of the β_2AR conformations in the MD simulations based on the ionic-lock distance is shown in Fig. 1 *B*–*E*. The results shown in Fig. 1 *B*–*E* are based on simulations initiated from step 74, where the ionic lock is initially in an inactive-like conformation with an ionic-lock distance of 13.2 Å at the beginning of the MD simulations, compared with the distance of 11 Å present in the inactive 5X7D crystal structure. In the simulation initiated with the agonist BI-167107, the distance is steadily progressing toward a more active-like conformation with an average distance of ~16 Å sampled toward the end of the simulation (Fig. 1*B*). In the simulation initiated with Carazolol, which initially assumes an ionic-lock distance of ~14.5 Å, the system undergoes a large shift in conformation at approximately 25-ns (Fig. 1*C*) sampling ionic-lock distances around 18 Å, similar to the distance of 19 Å observed in active-form crystal structure 3SN6. The associated conformations represent intermediate states with the average ionic-lock distance intermediate to the experimentally observed distances from the crystal structures indicated in Fig. 1 *B* and *C*. Subsequently, representative structures from

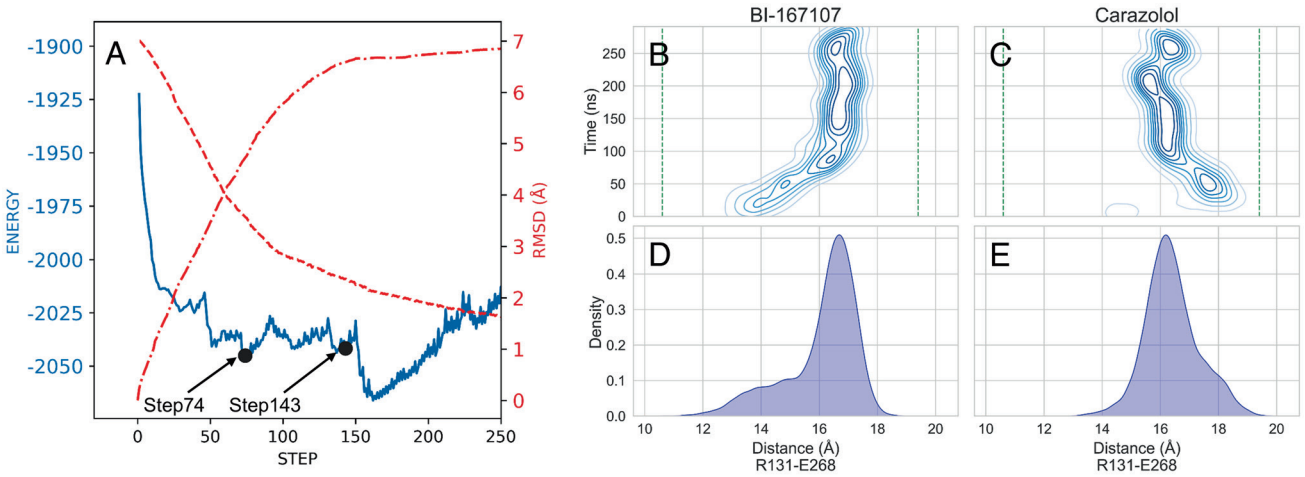

Fig. 1. Molecular dynamics simulations identified intermediate conformational states. (*A*) Climber Energy (kcal/mol) (blue line) and RMSD with respect to inactive (red dashed line) and active (red dash-dotted line) conformations (PDBIDs: 5X7D and 3SN6, respectively) during the morphing from the active to inactive form of β2AR. Black dots display the local energy minima along the morphing pathway selected for the two starting intermediate conformations. (*B*–*E*) Ionic-lock distance analysis from the MD simulations. (*B* and *C*) Time evolution of the ionic-lock distance from the MD simulations in the presence of BI-167107 or Carazolol, respectively. Green vertical dashed lines represent the ionic-lock alpha carbon distance measured from the inactive (~11 Å) and active (~19.5 Å) receptor. (*D* and *E*) Density distributions of the ionic-lock distance from the MD simulations in the presence of BI-167107 or Carazolol, respectively. The simulations in *B* and *C* were initiated from the Step74 conformation.

the MD simulations were selected using RMSD clustering for identifying conformations in which the ionic-lock distance corresponded to the average value from the MD simulations (Fig. 1 *D* and *E*). These structures were from simulations initiated from Climber step 74 individually initiated with BI-167107 and Carazolol, which will be referred to as Step74A and Step74B, respectively.

SILCS Allosteric Binding Site Identification. Identification of possible allosteric binding sites and subsequent database screening to identify putative AMs were performed using SILCS methodology (27, 28). SILCS simulations were performed to generate functional group affinity maps (referred to as FragMaps) for the intermediate β_2AR conformations, Step74A and Step74B. The SILCS method is based on Grand Canonical Monte Carlo (GCMC) MD simulations using an explicit aqueous environment that includes 8 solutes (35, 36). During the SILCS simulations, water and solutes, representative of different functional groups, compete around and throughout the entire protein, including cryptic pockets that are deep or totally inaccessible to the aqueous environment. Shown in Fig. 2*A* are the SILCS FragMaps overlaid on the Step74A conformation used to initiate the SILCS simulation. Evident are the apolar FragMaps around the TM region of the protein that occupy regions adjacent to the hydrophobic region of the bilayer, negative charged maps on the intracellular face of the receptors, particularly around the ends of TM helices 5 and 6, and the presence of apolar, hydrogen bond donor and acceptor, and positive FragMaps throughout the interior core of the receptor. These latter maps indicate the utility of the SILCS approach for identifying interior regions on the protein amenable to the binding of various functional groups. Identification of putative allosteric binding sites was done using the SILCS-Hotspots approach (30). This involved comprehensive docking of 101 mono- and bicyclic chemical fragments in the field of the FragMaps to generate fragment binding poses that encompass the entire protein. Two rounds of clustering were then performed from which final Hotspots that act as the basis for allosteric site identification were identified. Shown in Fig. 2*B* are the Hotspots on the Step74A conformer. The presence of Hotspots throughout the protein, including the surface and interior regions, is evident, consistent with the distribution of the FragMaps. Further in-depth visual inspection of the Hotspots was then undertaken to identify possible allosteric sites to which drug-like molecules would bind, potentially acting as AMs.

Allosteric site selection focused on the identification of collections of adjacent Hotspots in which fragments occupying those sites could potentially be linked to create drug-like molecules. In this process, emphasis is on the relative location of adjacent Hotspots and the presence of open regions between those hotspots based on SILCS exclusion maps, with the rank ordering of the Hotspots given lower priority, as described previously (30). In addition, sites located in the vicinity of the residues known to impact the activity of β_2AR were given priority. From this process, a site comprised of 3 Hotspots was identified. The site is present in both the Step74A and Step74B systems between helices 3, 5, 6, and 7 (Fig. 2*C* and *SI Appendix*, Table S1). While analysis of the solvent accessible surface in that region (Fig. 2*D*) shows minimal free space in the vicinity of those Hotspots as well as indicating the location of the binding site on the interior of the TM bundle of helices, analysis of the SILCS exclusion maps around the Hotspots (Fig. 2*E*) shows that the region between and around the Hotspots is accessible for accommodating larger ligands. The exclusion maps are defined based on the regions of the protein in which the water or solutes do not sample during the SILCS simulations and, therefore, represent the extent to which the protein can relax to allow ligand binding in contrast to a simple solvent accessible surface based on a single protein structure. Accounting for protein flexibility in the SILCS method clearly identifies regions that can become accessible thereby facilitating the identification of putative binding sites not evident in single modeled or experimental structures.

Allosteric Modulator Identification. In silico database screening to identify putative AMs that bind to the identified site initially involved screening using pharmacophores generated with the SILCS-PHARM approach (33). This approach involves generation of pharmacophore features in the vicinity of the selected Hotspots based on the FragMaps in combination with clustering of the voxels

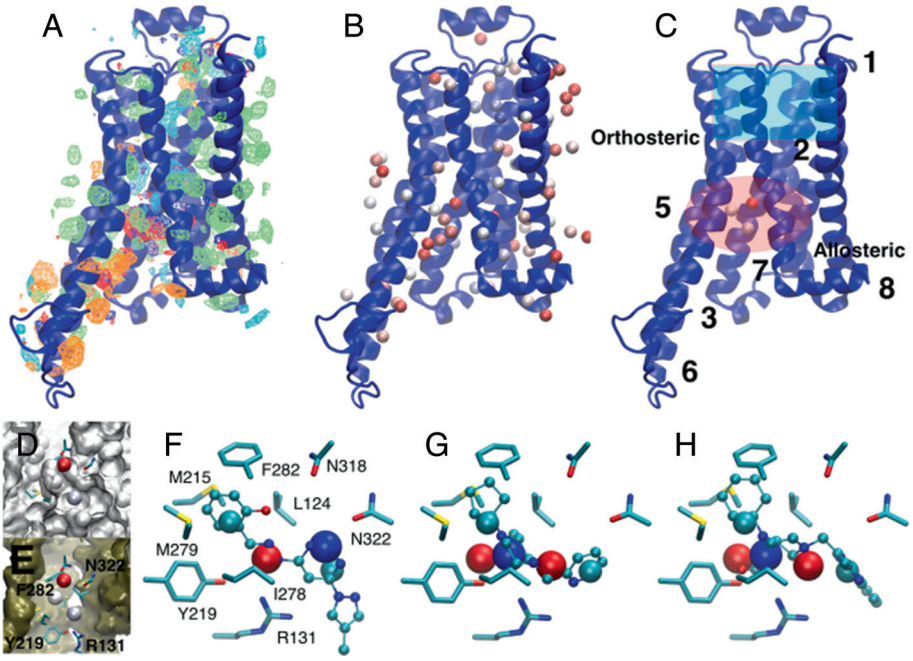

Fig. 2. SLICS approach identified an allosteric binding site on the β_2AR. Structure of the Step74 conformation used to initiate the SILCS simulations (blue, cartoon) along with (*A*) the SILCS FragMaps as mesh representations (apolar (green, −0.9), hydrogen bond donor (blue, −0.6) and acceptor (red, −0.6), negative (orange, −1.2) and positive (cyan, −1.2 kcal), where the energy indicates the isocontour cutoff in kcal/mol), (*B*) SILCS-Hotspots throughout the entire protein (VDW spheres, scaled by 0.7, colored by LGFE score from red to blue for the most favorable to least favorable ranked Hotspots) and (*C*) 3 Hotspots selected that define the identified allosteric site (red transparent oval) located below the orthosteric site (cyan transparent rectangle) between helices 3, 5, 6, and 7 (TM helix numbers shown except 4, which is on the back of the image). (*D* and *E*) Step74 structure in the region of the allosteric binding site showing residues defining the site (sticks, atom colored) and 3 selected Hotspots in the presence of the (*D*) Solvent Accessible Surface (white) or (*E*) SILCS Exclusion Map (tan). Compounds shown in *F*, *G*, and *H* are the SILCS-docked orientations of positive or negative allosteric modulators (*F*) 36, (*G*) 37, and (*H*) 42 (CPK, atom colored) overlaid on the side chains of the residues defining the allosteric binding site (stick, atom colored) and the pharmacophores used to select the respective compounds (VDW spheres, hydrophobic (cyan), hydrogen bond acceptor (red), and hydrogen bond donor (blue)). The pharmacophores in panels G and H are identical. Residue numbers in F are based on the Ballesteros nomenclature (PDB IDs shown in *SI Appendix*, Table S1).

that define the different FragMaps. From these pharmacophore features, 8 pharmacophore hypotheses were selected for database screening, with each containing 4 or 5 pharmacophore features.

Two example pharmacophores that ultimately identified allosteric modulators are shown in Fig. 2 *F*–*H*, respectively, along with the amino acid side chains lining the putative binding pocket (labeled in Fig. 2*F* and *SI Appendix*, Table S1). The complementarity between the pharmacophore features and the adjacent amino acids is evident. For example, the right side of 2F shows a hydrophobic feature (cyan sphere) surrounded by two Met, a Phe, and a Leu residue. Interestingly, adjacent to R131 is a hydrogen bond acceptor feature indicating that despite the positive charge of R131, a negative functional group on a ligand in that region is not highly favored.

Pharmacophore screening using Pharmer (37) produced up to 10,000 hits/pharmacophore based on RMSD of the ligand functional groups with respect to the pharmacophore features. The selected compounds were then pooled and subjected to local optimization and scoring using SILCS–MC pose refinement from which the Ligand Grid Free Energy (LGFE) scores were calculated. From this step, the top 1,000 compounds were selected. These compounds were then subjected to chemical fingerprint clustering and bioavailability analysis using the 4D-Bioavailability metric (38) from which a total of 100 chemically diverse compounds were selected for purchase from the commercial vendor. All the 100 compounds were successfully obtained and subjected to biological evaluation yielding 8 lead compounds that modulated the activation of β_2AR (*SI Appendix*, Fig. S1). Of these, 5 where PAMs and 3 were NAMs as described below. The predicted bound conformation of the 3 AMs subjected to comprehensive experimental validation is included in Fig. 2 *F*–*H*.

Lead Compounds Modulate Agonist-Induced cAMP Generation. Activation of β_2AR by orthosteric ligands leads to activation of Gαs subunit, which in turn activates adenylyl cyclase (AC) to hydrolyze ATP to produce cAMP (39). To determine the biological activity of the AMs of the β_2AR, HEK293 cells overexpressing human wild-type β_2AR were stimulated with different concentrations of test compounds and evaluated for cAMP production using a cAMP ELISA. None of the compounds tested promoted cAMP accumulation in HEK293 cells (Fig. 3*A*). However, when cells were treated with varying concentrations of test compounds along with 100 nM isoproterenol (ISO), the PAMs and NAMs modulated ISO-induced cAMP generation in a dose-dependent manner (Fig. 3*B*). All subsequent studies were carried out using AMs at 100 nM based on these dose–response studies. Further, treatment of HEK293 cells with ISO increased cellular cAMP levels in a concentration-dependent manner (Fig. 3*C*). Costimulation with ISO and 100 nM of different AMs significantly increased or decreased the dose-dependent effect of ISO on cAMP accumulation (Fig. 3*C* and *SI Appendix*, Fig. S3). Biological evaluation of obtained compounds yielded 8 compounds that modulated the activation of β_2AR. Of these, compound 37 was the most effective PAM and compounds 36 and 42 were the most effective NAMs (Fig. 3*C* and *SI Appendix*, Fig. S3). These compounds were used in subsequent studies. EC_{50} and E_{max} values of ISO alone or in combination with PAMs and NAMs are depicted in Table 1.

To evaluate the observed modulating effects of PAMs and NAMs on β_2AR-Gs-cAMP signaling in a physiologically relevant system, we further tested the effect of the compounds in primary human ASM cells, which express β_2AR endogenously. Concomitant

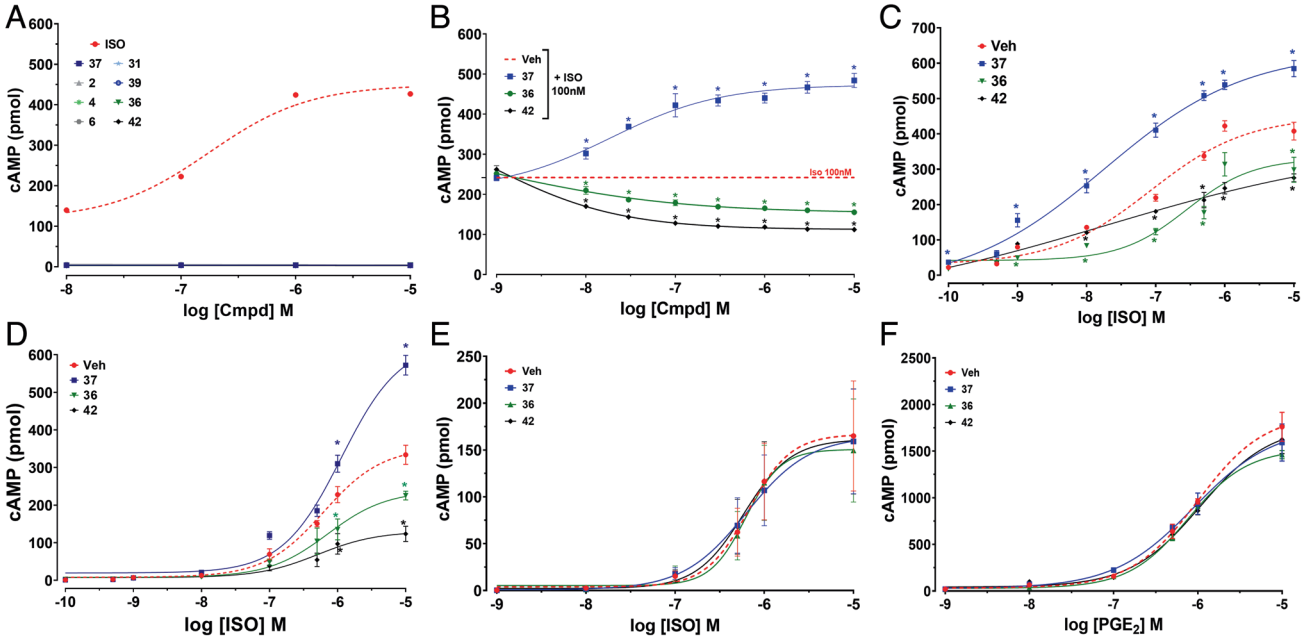

Fig. 3. Effect of β_2AR modulators on agonist-induced cAMP accumulation. Cells were plated into a 24-well plate and stimulated with vehicle or β_2AR modulators in combination with isoproterenol (ISO) for 10 min and cAMP accumulation was measured by ELISA as described in *Methods*. Isoproterenol (ISO)/ β_2AR modulators dose–response curve was generated using nonlinear (4-parameter) logistic curve from multiple experiments (n = 6). All statistical significances were determined using a two-way ANOVA with Bonferroni post hoc analysis. (*A*) HEK293 cells expressing β_2AR were stimulated with different concentrations of AMs or ISO. (*B*) HEK293 cells expressing β_2AR were stimulated with different concentrations of AMs and 100 nM ISO. Further, top ranking PAM and NAMs (100 nM) were used to stimulate (*C*) HEK293 cells and (*D*) human ASM cells in combination with different concentrations of ISO. n = 5–8, $*P < 0.05$ (compound vs. ISO). (*E*) cAMP generation was assessed in HEK293 cells expressing human β_1AR stimulated with varying concentrations of ISO ± 100 nM AMs. n = 6. (*F*) Human ASM cells were stimulated with different concentrations of prostaglandin E_2 with vehicle or 100 nM AMs and cAMP was assessed. n = 5. Error bars represent ± SEM.

treatment of human ASM cells with PAMs or NAMs enhanced or attenuated ISO-induced cAMP generation, respectively (Fig. 3*D* and *SI Appendix*, Fig. S3). EC_{50} and E_{max} values of ISO-induced cAMP generation in human ASM cells are given in Table 1.

AMs are Specific for β_2AR. In order to establish the specificity of the AMs to β_2AR, we tested the effect of AMs on ISO-induced cAMP generation in HEK293 cells expressing human β_1AR. AMs did not modulate ISO-induced cAMP generation in HEK293 cells expressing β_1AR (Fig. 3*E*). Further, in human ASM cells, which express Gs-coupled EP2 and EP4 receptors, PAMs or NAMs did not modulate prostaglandin E_2-induced cAMP generation (Fig. 3*F*). Collectively, these findings suggest the specificity of the AMs to β_2AR.

Lead Compounds Do Not Affect β-Agonist-Induced Recruitment of β-Arrestins. In addition to the canonical Gs signaling, the "balanced" β-agonists induce β-arrestin recruitment to the β_2AR resulting in β_2AR desensitization and activation of noncanonical signaling such as ERK1/2 signaling (1). Therefore, we aimed to determine the effect of compounds 37, 36, and 42 on ISO-induced β-arrestin2 recruitment to the β_2AR using a well-established bioluminescence resonance energy transfer (BRET) assay (40). ISO treatment of HEK293 cells expressing β_2AR resulted in a dose-dependent increase in recruitment of β-arrestin2 to the receptor (Fig. 4). Concomitant treatment of cells with either PAM or NAMs did not alter ISO-mediated changes in BRET (Fig. 4). Furthermore, we tested the effect of AMs on ISO-induced phosphorylation of ERK1/2; neither PAM nor NAMs altered ERK1/2 phosphorylation in HEK293 (Fig. 4*B*) or ASM cells (*SI Appendix*, Fig. S4). These data suggest that increased β_2AR-Gs signaling effected by the small molecule PAM occurs without alterations in β-arrestin recruitment to the β_2AR, or noncanonical β-arrestin-dependent signaling induced by orthosteric β-agonist.

AMs Do Not Modulate Binding of Orthosteric Agonist to β_2AR. PAMs or NAMs have the potential to influence β_2AR signaling by altering the affinity of the orthosteric ligand to β_2AR. Therefore, we tested the effect of AMs on the binding affinity of ISO to β_2AR using a well-established radiolabel ligand binding assay. AMs did not alter binding affinity of ISO to the β_2AR (Fig. 5 *A–D*).

Mutagenesis Studies Confirm the Mechanism of Action of Lead Compounds. To validate the identity of the computationally identified allosteric site, we generated β_2AR containing R131K, R131A, Y219F, Y219S, Y219A, F282Y, F282W, and F282A mutations (Fig. 6*A*). Wild-type and mutant β_2AR were expressed in HEK293 cells, and ISO-induced cAMP generation was measured in the presence or absence of the PAM compound 37, or NAM compounds 36 and 42 (Fig. 6 *B–E*). The compounds were also tested at different concentrations of ISO in the cells expressing mutant β_2AR (*SI Appendix*, Fig. S5). The cAMP response was enhanced in cells expressing R131A and diminished in F282A mutant β_2AR compared with cells expressing wild-type β_2AR. The ISO-induced cAMP generation in cells expressing wild-type and Y219A mutant β_2AR was comparable (*SI Appendix*, Fig. S5*A*). Further, as expected, compound 37 enhanced ISO-induced cAMP generation in cells expressing wild-type β_2AR, and this effect was abolished in cells expressing mutant β_2AR (Fig. 6 *C–E* and *SI Appendix*, Fig. S5 *B–D*). Furthermore, NAM compounds 36 and 42 inhibited ISO-induced cAMP generation in wild-type β_2AR expressing cells, and this inhibition was attenuated in cells expressing R131K, R131A, Y219F, Y219S, Y219A, F282Y, F282W, and F282A mutant β_2ARs (Fig. 6 *C–E*

Table 1. Effect of β_2AR modulators on cAMP accumulation

Compound	EC_{50} [nM]	Emax [pmol] raw values	Emax [%] normalized to veh
A. HEK293 Cells			
37	18.76 ± 7.03	643.7 ± 36.25*	143.17 ± 5.63*
2	22.45 ± 9.04	432.96 ± 27.74	128.4 ± 13.64
31	105.69 ± 69.6	510.53 ± 68.64	113.55 ± 13.45
4	97.64 ± 63.23	577.3 ± 78.72	101.15 ± 8.01
Veh	84.4 ± 21.95	449.62 ± 22.31	100
39	15.58 ± 6.14	410.95 ± 21.65	91.4 ± 5.27
42	18.75 ± 30.99	374.64 ± 121.89	83.32 ± 32.53
6	50.09 ± 23.01	454.79 ± 36.42	77.87 ± 14.57
36	281.66 ± 108.3*	330.13 ± 33.48	73.42 ± 10.14
B. Human ASM cells			
37	1139.29 ± 146.68	633.85 ± 23.43*	178.93 ± 3.7*
2	750.49 ± 168.88	448.43 ± 28.77	126.59 ± 6.42
4	524.25 ± 141.8	406.67 ± 29.16	114.8 ± 7.17
39	404.31 ± 115.82	400.63 ± 29.06	113.09 ± 7.25
Veh	618.66 ± 108.67	354.25 ± 16.72	100
6	307.54 ± 96.85	339.18 ± 24.63	95.75 ± 7.26
36	714.33 ± 235.5	238.42 ± 21.43*	67.3 ± 8.99*
31	120.52 ± 48.54	227.42 ± 16.74*	64.2 ± 7.36*
42	513.17 ± 275.92	130.25 ± 17.46*	36.77 ± 13.41*

EC_{50} and E_{max} for cAMP accumulation in (A) HEK293 and (B) human ASM cells stimulated with different concentrations of ISO in the presence of vehicle or 100 nM AMs were calculated using non-linear regression curve on GraphPad Prism software. Values represent mean ± SEM from n = 5–8.
*P < 0.05 (compound + ISO vs. Veh + ISO) using One-Way ANOVA with Dunnet post hoc analysis.

and *SI Appendix*, Fig. S5 *B–D*). Collectively, these findings demonstrate the critical requirement of amino acids R131, Y219, and F282 of the β_2AR in forming the binding pocket of PAMs and NAMs.

Mutagenesis of the β_2AR may influence the expression and translocation of the β_2AR to the cell surface. Therefore, to further validate the mutagenesis experiments, we assessed the cell surface expression of HA-tagged wild-type and mutant β_2AR using cell surface ELISA, as described previously (41). Baseline cell surface expression of different mutants of the β_2AR was similar to that of wild-type β_2AR (*SI Appendix*, Fig. S6).

Lead Compounds Do Not Alter β-Agonist-Induced Loss of β_2AR Cell Surface Expression. Previous studies have shown that stimulation of β_2AR with orthosteric ligands results in concentration- and time-dependent loss of cell surface expression of β_2AR (42). Therefore, we next tested the effect of the PAM or NAMs on the β-agonist-mediated loss of cell surface expression of the β_2AR. Treatment of HEK293 cells with ISO (100 nM) for 15 min resulted in a loss of cell surface expression of the β_2AR (*SI Appendix*, Fig S6*B*). Treatment of cells with PAM 37 or NAMs 36 and 42 in combination with ISO did not affect the ISO-induced loss of cell surface expression of wild-type or mutant β_2AR (*SI Appendix*, Fig S6*B*).

Lead Compounds Augment β-Agonist-Induced ASM Relaxation. β-agonists are the drug of choice for the management of acute bronchoconstriction in asthmatics, acting on the target ASM cells. The Gs-cAMP-protein kinase A signaling axis effected by β-agonists inhibits contraction of ASM cells via multiple mechanisms (1, 43). We therefore examined whether the modulation of this signaling pathway by the discovered PAM/NAMs translated into functional differences in β_2AR control of ASM contraction. In a standard gel-contraction assay, the collagen gels containing human ASM cells were incubated with different concentrations of ISO with vehicle or 100 nM AMs for 10 min, followed by stimulation with 10 μM histamine. The gel images were obtained before and after treatment with different agonists using an EVOS microscope, and a change in the gel area was calculated. Treatment with 10 μM histamine decreased the area of the gels, consistent with contraction of ASM cells. Pretreatment of gels with ISO inhibited the histamine-induced decrease in gel area (Fig. 7*A*). Pretreatment of gels with ISO in combination with compound 37 significantly enhanced, whereas compounds 36 and 42 either slightly reduced or had no effect, on ISO-mediated inhibition of histamine-induced contraction of human ASM cells (Fig. 7*A*).

To further examine the effect of PAMs and NAMs on β-agonists-mediated regulation of bronchorelaxation in a physiologically relevant model, we used human and murine precision-cut lung slices. Treatment of lung slices with the contractile agent methacholine resulted in the narrowing of airways. Lung slices were treated with increasing concentrations of ISO plus either vehicle or 100 nM of compounds 37, 36, or 42, and a change in airway lumen area was determined. Treatment with ISO alone resulted in a dose-dependent increase in airway lumen area (bronchodilation). This effect was significantly enhanced in the presence of 100 nM compound 37 and mitigated in the presence of compounds 36 and 42 (Fig. 7 *B* and *C* and *SI Appendix*, Fig. S7); the other AMs tested had varying effects of ISO-induced bronchodilation in murine lung slices (*SI Appendix*, Fig. S7). The EC_{50} and E_{max} values for ISO-mediated relaxation of murine and human lung slices are presented in Table 2.

Collectively, these results from cell- and tissue- based models of ASM contraction strongly suggest that PAM properties of compound 37 extend to β_2AR-Gs function (bronchodilation), with the potential to be exploited therapeutically.

Discussion

Presented is a combined computational and experimental study to identify allosteric modulators of the β_2AR, which offer the potential of improved therapeutic efficacy in the management of obstructive lung diseases such as asthma. We utilized the computational SILCS approach to identify previously unidentified putative ligand-binding sites that would potentially act as allosteric sites. To facilitate the identification of such sites, intermediate conformations of β_2AR, with respect to the active and inactive conformations of the protein, were generated using the program Climber followed by MD simulations of the receptor in its apo form or in complex with BI-167107 or Carazolol. SILCS-Hotspots analysis on the selected conformations identified a putative allosteric binding pocket on the interior of the receptor, adjacent to the ionic lock, suitable for the binding of drug-like molecules. Subsequently, a combination of SILCS-Pharmacophore, Pharmer and SILCS–MC pose refinement programs was used to identify a collection of chemically diverse, commercially available compounds with suitable physiochemical properties as required for experimental studies. From this list, a total of 100 compounds were obtained and subjected to experimental evaluation. Among these, eight compounds modulated β-agonist-induced cAMP generation in HEK293 cells expressing β_2AR with no effect on the recruitment of β-arrestins to the β_2AR. In primary human ASM cells expressing endogenous β_2AR, the lead compounds enhanced β_2AR-mediated Gs signaling as measured by ISO-induced cAMP generation. Importantly, a lead PAM 37 enhanced ISO-induced relaxation of human ASM cells and bronchodilation of human and murine airways ex vivo. Our study demonstrates that PAM

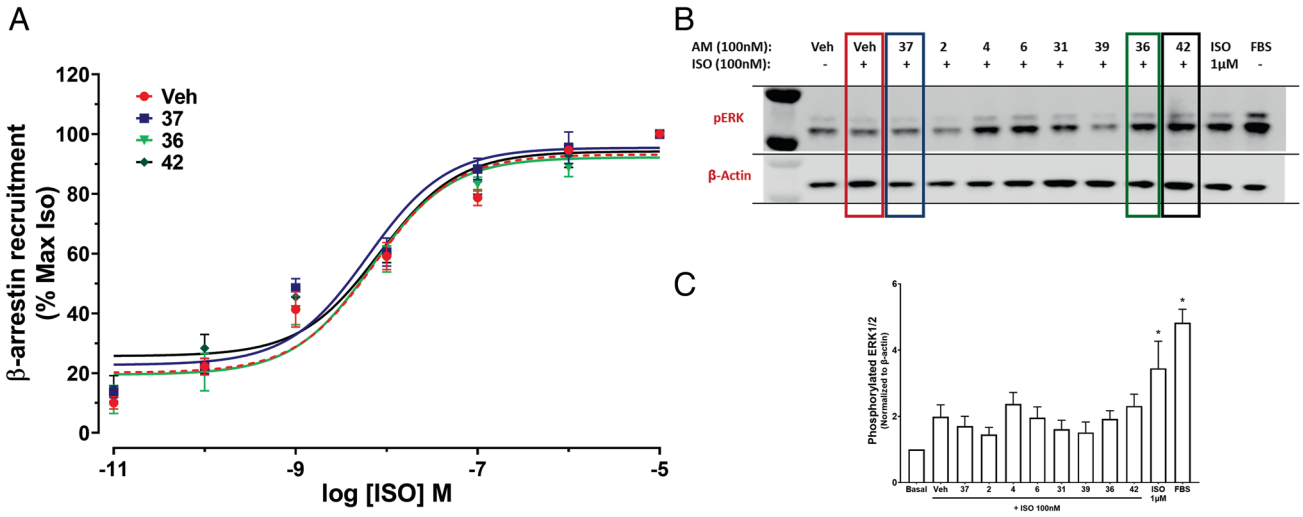

Fig. 4. Effect of β_2AR modulators on isoproterenol-induced β-arrestin recruitment and phosphorylation of ERK1/2. (*A*) Cells expressing BRET reporters (Rluc-β_2AR and GFP-β-arrestin2) were treated with vehicle or 100 nM AMs with increasing concentrations of ISO and change in fluorescence was measured using a plate reader. ISO treatment enhanced recruitment of β-arrestin to the receptor, and cotreatment of cells with AMs did not increase isoproterenol-induced β-arrestin recruitment to the β_2AR (n = 5). Error bars represent ± SEM. Graphpad Prism was used to generate nonlinear regression curves (4-PL) and a two-way ANOVA with Bonferroni post hoc was used for statistical analysis. (*B*) ISO-induced activation of β-arrestin-ERK1/2 was assessed by western blotting and (*C*) band intensities were normalized to β-actin. Data are expressed as fold change from vehicle-treated cells. AMs (100 nM) did not further modulate 100 nM ISO-induced phosphorylation of ERK in HEK293 cells. n = 4 *$P < 0.05$ ISO vs. AMs + ISO using Student's *t* test. Error bars represent ± SEM (*B* and *C*).

compound 37 selectively augments canonical β_2AR-Gs-cAMP signaling that translates into superior β-agonist-mediated bronchorelaxation. AMs do not directly modulate the binding affinity of the orthosteric β-agonist to the receptor. Alternately, the AMs might function by stabilizing the intermediate β_2AR confirmations thus keeping the receptor active for longer. Their interactions with an intermediate conformation may also explain their lack of impact on the affinity of the orthosteric β-agonist ISO.

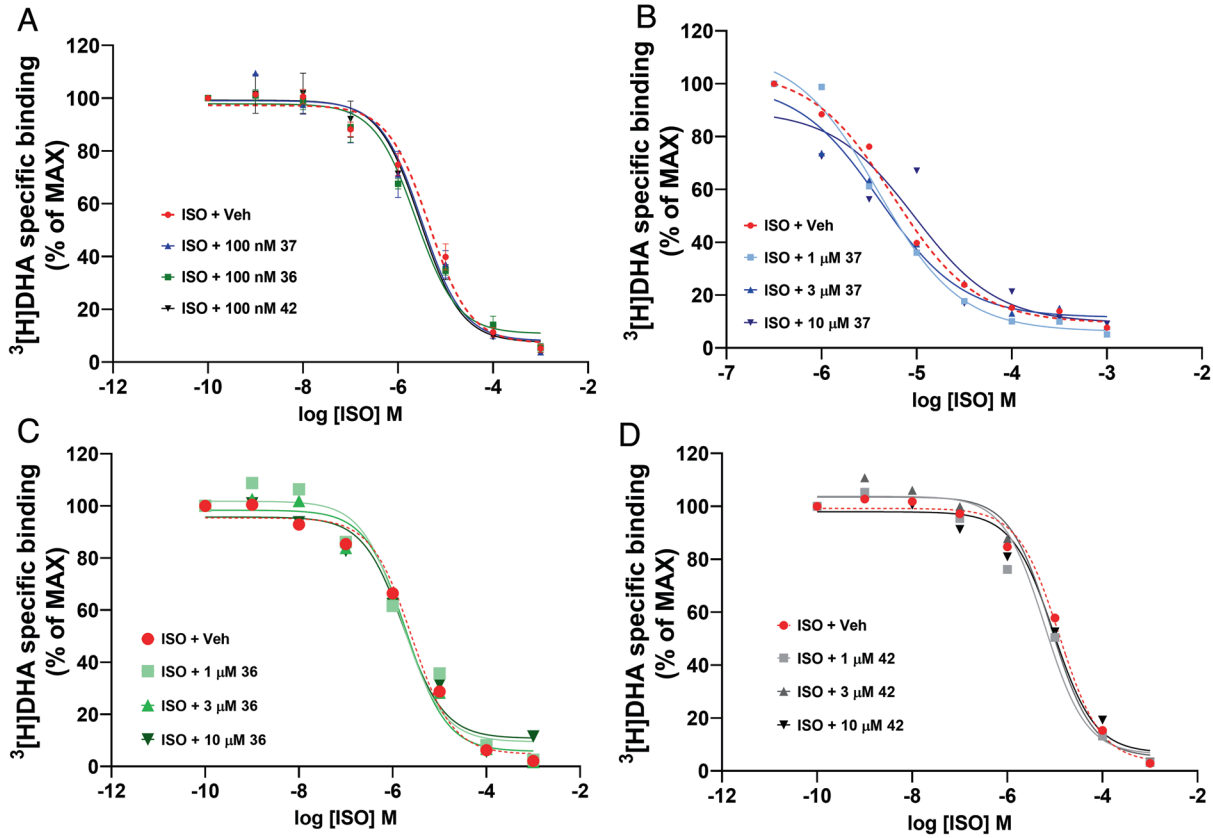

Fig. 5. Effect of AMs on the binding affinity of ISO to the β_2AR. Cell membranes expressing the β_2AR were incubated with 3 nM [^{3}H]DHA and with increasing concentrations of ISO in the presence or absence of AMs. Nonspecific binding was assessed with 10 μM alprenolol. Binding competition curves were generated using the function log(inhibitor) vs. response (three parameters) of the nonlinear regression curve fitting in GraphPad Prism and are represented as percentage of the maximal [^{3}H]DHA-specific binding. (*A*) Compounds 37, 36, and 42 were tested at 100 nM concentration and (*B*–*D*) subsequently, each of the compounds was tested at different concentrations. n = 4. Error bars represent ± SEM.

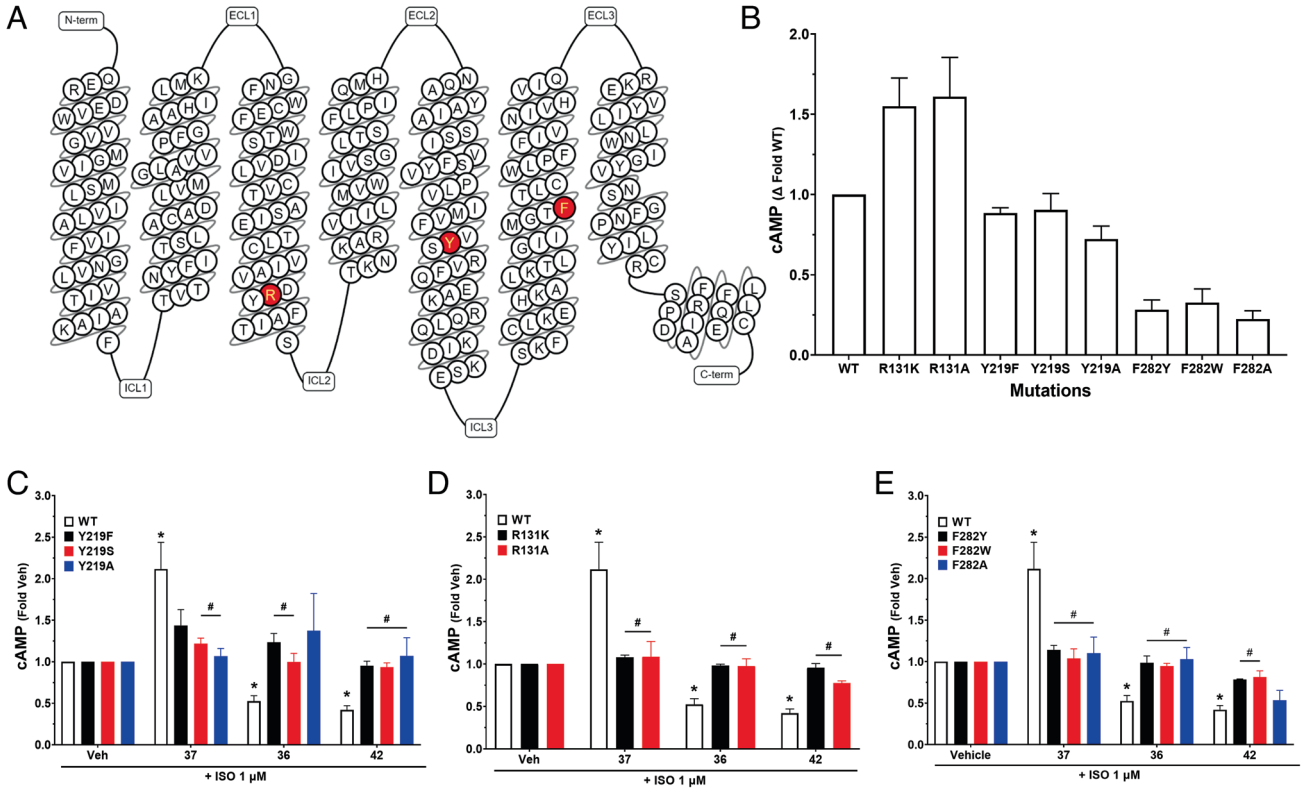

Fig. 6. Identification of the allosteric modulator binding site on the β_2AR. Amino acids forming the putative binding pocket for the AMs on β_2AR identified by SLICS computational modeling are shown in *(A)*. Wild-Type (WT) and mutant β_2AR were expressed in HEK293 cells, and cAMP accumulation was measured upon stimulation with 1 μM ISO (*B*). Cells were costimulated with vehicle or β_2AR modulators (100 nM) and ISO (1 μM) for 10 min, and cAMP accumulation was measured in cells expressing wild-type and Y219 (*C*), R131 (*D*), and F282 (*E*) mutant β_2AR (n = 3–4, *P < 0.05 Compound + ISO vs. Veh + ISO, #P < 0.05 WT vs. β_2AR mutant). Student's *t* test was used to determine statistical significances. Error bars represent ± SEM.

Computational Approach to Allosteric Binding Site Identification. SILCS is a cosolvent molecular simulation approach that maps the functional group affinity pattern of a protein, including the protein interior, taking into account protein flexibility as well as protein and functional group desolvation contributions. Notably, the SILCS-Hotspots method allows for docking a collection of fragments on the entire protein to identify putative binding sites suitable for drug-like molecules (30) in a highly computational efficient fashion with a level of accuracy comparable with other state-of-the-art computational methods such as free energy perturbation (44). The present results further represent the capability of the SILCS method to identify allosteric binding sites showing, notably, its utility against a GPCR (30, 32, 35). The technology takes advantage of the inclusion of protein flexibility in SILCS combined with the use of GCMC water and solute sampling to identify possible binding sites on the interior of a protein not evident in experimental crystallographic or cryo-EM structures. Further improvements in the SILCS approach may include enhancement of the conformational sampling of the protein, possibly through increasing the simulation temperature, as well as generating additional intermediate conformations of the GPCR. The latter could be achieved through a number of enhanced sampling simulation technologies (45).

Our study identified a previously unidentified allosteric site on the β_2AR comprised of amino acids R131, Y219, and F282. The SILCS-Hotspots-identified allosteric binding site (Fig. 2 *B* and *C*) is located roughly 20 Å below the orthosteric binding site inside the TM bundle. The Hotspots that make up the site were of interest as they are located just below the PIF connector motif (P211, I121, and F282) (46) and extend out toward the core of the TM bundle. This central site is completely inaccessible in the inactive conformation as it is occupied by TM helix 6. However, in the intermediate conformation identified using Climber and in the conformations sampled during the subsequent MD simulations, R131 shifts up toward the site previously occupied by helix 6 that has been observed in an experimental structure of the activated receptor (47). Further, our findings suggest that mutation of R131 enhances ISO-induced cAMP accumulation (*SI Appendix*, Fig. S5*A*) consistent with the previously published literature (48, 49). Mutation in F282 on the contrary attenuated ISO-induced cAMP generation similar to what has been shown previously (48). The cAMP generation in cells expressing Y219A mutant receptor was comparable with the wild-type receptor. Importantly, the AMs did not have any effect on ISO-induced cAMP generation in cells expressing mutant β_2AR supporting our hypothesis that AMs potentially bind to a pocket formed by these three amino acids (Fig. 6 *C*, *D* and *E* and *SI Appendix*, Fig. S5 *B*, *C* and *D*). Further, cell surface expression ELISA findings demonstrated that AMs do not modulate ISO-induced internalization of the β_2AR. A previous study demonstrated that mutation in Y219 renders the β_2AR resistant to agonist-induced desensitization and internalization (50). However, we observed an ISO-induced loss of cell surface expression with the Y219 mutant, mostly likely due to significant differences in experimental approach including different cell systems, which are known to produce variable results in studies of β_2AR regulation (51).

Notably, the present site does not correspond to a previously identified allosteric sites on β_2AR. The first identified β_2AR modulator, a NAM, binds to the intracellular termini of TM helices 1, 2, 6, and 7 (21). A PAM (Cmpd 6), binds to a pocket formed by ICL2 and TM helices 3 and 4 (23) and more recently, a NAM was identified and shown to bind to TM helices 3 and 5 (22).

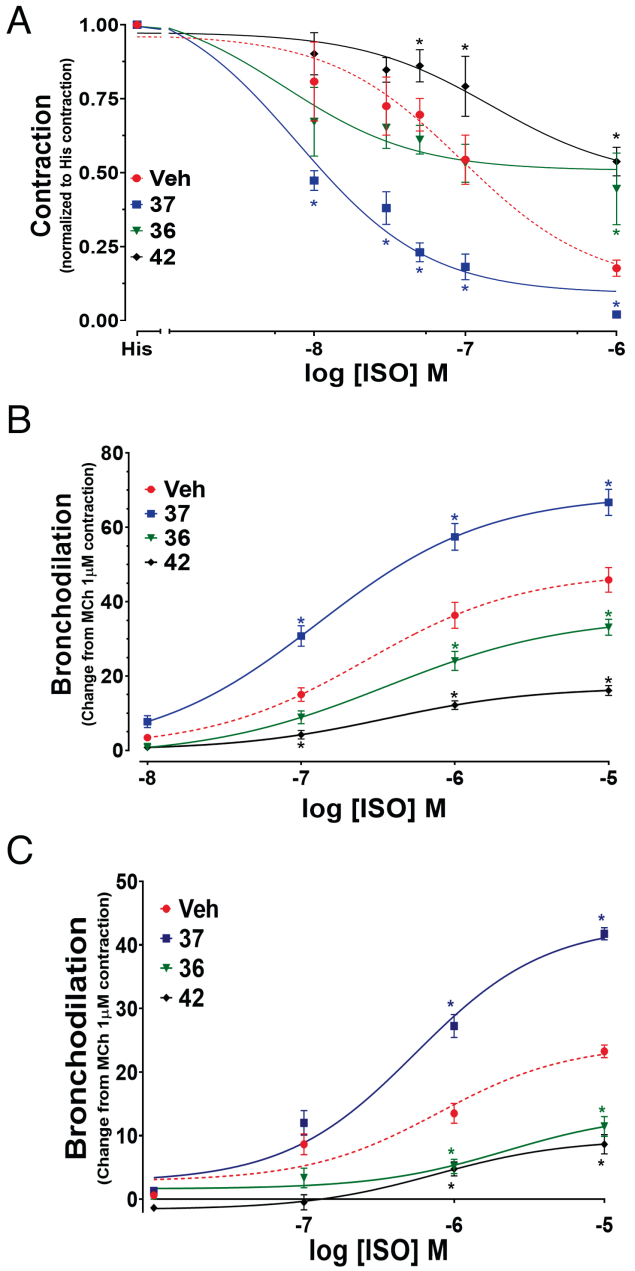

Fig. 7. Effect of allosteric modulators on β-agonist-mediated inhibition of contraction of human ASM cells and augmentation of bronchodilation in human and murine lung slices. (*A*) Collagen gels containing human ASM cells were pretreated with veh or AMs (100 nM) and different concentrations of ISO for 10 min and stimulated with histamine (10 μM). Images of collagen gels were taken at 10-min intervals over 30 min and normalized to the basal area for each measure. Data are representative of n = 6–10 independent donors. **P* < 0.05 His vs. ISO + His, #*P* < 0.05 Veh + ISO vs. Compound + ISO. His, histamine. (*B*) Human and (*C*) murine lung slices were contracted with methacholine (1 μM) for 10 min and treated with vehicle or β_2AR modulators (100 nM) for 10 min followed by treatment with an increasing concentration of ISO. Change in lumen area of airways was used to determine the magnitude of bronchodilation. n = 8, **P* < 0.05 Veh + ISO vs. Compounds + ISO. Nonlinear curve fitting (Inhibitor vs. three-parameter for *A* and agonist vs. four-parameter logistic curve fit for *B* and *C*) was generated using Graphpad Prism software. All statistical differences were analyzed using a two-way ANOVA with Bonferroni post hoc analysis. Error bars represent ± SEM.

Interestingly, these two allosteric sites (21, 22) are located on the protein-membrane interface and may potentially modulate the receptor response from the membrane side by impacting G-protein binding or by disrupting the polar network around the activation switch and thus stabilizing the inactive receptor conformation.

Table 2. Bronchodilation of precision cut lung slices

Compound	EC_{50} [nM]	E_{max} raw values	E_{max} [%] normalized to veh
A. Human PCLS			
37	129.36 ± 54.84	68.86 ± 5.16*	143.64 ± 7.49*
Veh	266.89 ± 114.55	47.94 ± 4.51	100
36	355.97 ± 174.79	36.06 ± 4.78	75.23 ± 13.26
42	354.75 ± 175.99	16.9 ± 1.94*	35.26 ± 11.47*
B. Murine PCLS			
37	551.88 ± 134.33	43.23 ± 1.91*	177.33 ± 4.42*
4	1128.57 ± 404.04	39.02 ± 3.05*	160.05 ± 7.82*
2	509.18 ± 198.49	37.84 ± 2.56*	155.23 ± 6.76*
6	231.51 ± 72.04	24.63 ± 1.16	101.03 ± 4.73
Veh	788.67 ± 328.16	24.38 ± 1.96	100
39	834.19 ± 391.81	24.11 ± 2.17	98.89 ± 9.02
31	174.56 ± 66.73	21.35 ± 1.12	87.58 ± 5.24
36	2203.36 ± 1827.42	13.56 ± 2.62*	55.62 ± 19.29*
42	749.99 ± 463.84	9.42 ± 1.47*	38.64 ± 15.63*

EC_{50} and E_{max} of ISO for bronchodilation of (A) human and (B) murine precision cut lung slices in the presence of vehicle or AMs (100 nM) were calculated using nonlinear regression curve on GraphPad Prism software. Values represent mean ± SEM from n = 5–8. **P* < 0.05 (compound+ISO vs. Veh+ISO) using One-Way ANOVA with Dunnet post hoc analysis.

Concerning the activity of the present allosteric modulators, the location of the site is below the orthosteric site in a deep pocket in the central region of the TM helices (Fig. 2 *D* and *E*). Shown in *SI Appendix*, Fig. S2 of the Supplement are bound orientations of 36, 37, and 42 along with the SILCS FragMaps further demonstrating the compounds' ability to participate in favorable interactions with the binding site. The similar orientations of the compounds and location of the allosteric site along with the lack of large changes in the EC_{50} values for ISO in the experiments assessing cAMP generation (Fig. 3 and Table 1), indicates that the mechanism of action would be to stabilize specific conformations of the receptor rather than directly impacting the binding of agonists to the orthosteric site. This would involve a shift in the conformations toward more or less active conformations based on the details of the specific interactions of the compounds with the region around the binding site given that both PAMs and NAMs have been identified. In addition, these changes would impact G protein interactions over those with β-arrestin based on the arrestin recruitment experiments (Fig. 4). Further, our radioligand binding data suggest that AMs do not modulate orthosteric ligand binding affinity on β_2AR (Fig. 5) unlike other β_2AR allosteric modulators that have been described in the literature, probably because the AMs identified in our study bind to an intermediate conformation as opposed to a fully activated conformation of β_2AR to which the other known allosteric modulators bind. However, further details of the mechanism will require detailed structural and computational biology analyses.

Biological Effects of PAM and NAM and Clinical Significance. It is well-appreciated that the therapeutic efficacy of β-agonists involves complex interplay of interaction between the β_2AR and G proteins, kinases, and β-arrestins (7–9). GRKs and β-arrestins are key regulatory molecules involved in agonist-specific desensitization of numerous GPCRs, limiting the capacity of receptor to maintain signaling, and the associated functional consequences. β-agonists are used as both prophylaxis and treatment for asthma, based on their ability to reverse bronchoconstriction caused by ASM contraction. Yet chronic β-agonist use by asthmatics is associated with a loss of drug efficacy, including a loss of bronchoprotective effect, and worsening of asthma control (2, 5, 52, 53). Studies

using ASM cells and murine models of asthma, strongly implicate GRK- and β-arrestin- mediated β_2AR desensitization in the loss of bronchoprotection by β-agonists, as molecular and genetic strategies targeting these regulatory molecules augment and sustain β_2AR-stimulated cAMP and PKA signaling, while increasing β_2AR-agonist-mediated ASM relaxation and bronchorelaxation (9, 10). In addition, numerous recent studies have also implicated β-arrestin2 in promoting β_2AR-dependent development of the asthma phenotype in murine models of asthma presumably via noncanonical β_2AR signaling that occurs via the formation of a β-arrestin2 scaffold (11, 54). Thus, identification of agents that help overcome the constraints imposed by GRKs/arrestins represents exciting therapeutic candidates.

Augmenting Gs-cAMP signaling by β_2AR would potentially provide therapeutic benefit. In this regard, to a limited extent, phosphodiesterase inhibitors can augment canonical β_2AR-cAMP signaling. Yet their use in asthma appears to have limited efficacy and is complicated by significant off-target effects (54, 55). PAMs provide an alternative means of augmenting β_2AR-cAMP signaling. While one other β_2AR PAM has been reported to date, its characterization has been largely limited to signaling studies of HEK293 cells (22, 25, 26). In this study, we identified PAMs that increase cAMP signaling transduced by ISO in human ASM cells. Considering the endogenous level of β_2AR expression in human ASM the modulatory effects of AMs are different in ASM cells compared with that observed in the HEK293 cells. Consistent with our previous studies establishing the functional consequences of increasing ASM β_2AR-cAMP signaling, compound 37 significantly increased the ISO-induced relaxation of contracted human ASM cells and human and murine airways. Our study provides a proof-of-concept that ligands binding to a unique allosteric site on the β_2AR, can modulate cAMP signaling in ASM cells. This finding has wide-ranging implications given the prominent role of canonical β_2AR-Gs-cAMP in regulating cellular functions in multiple organ systems.

Coinciding with the promotion of Gs-cAMP signaling, interaction of agonist-occupied β_2AR with GRKs results in phosphorylation of the receptor and recruitment of arrestins followed by desensitization of β_2AR and activation of noncanonical signaling. Given activation of arrestin-mediated signaling by β-agonists is dose- and time-dependent, the ability of PAM to achieve a Gs-mediated relaxation at a lower β-agonist concentration is desirable. For these reasons, molecules that bias β_2AR signaling toward Gs without affecting β-arrestin recruitment could potentially limit/avoid problems demonstrated with use of balanced β-agonists.

In summary, our study identifies a allosteric binding site on the β_2AR activation of which selectively enhances canonical Gs-cAMP signaling in both cell lines transduced with β_2AR and physiologically relevant cells. Importantly, such signaling modulation translates into increased β_2AR function in ASM cells and tissues, rendering compound 37 and similar PAMs promising therapeutic tools in the management of obstructive lung diseases.

Materials and Methods

Computational Methods. A detail description of the computational methods is presented in the *SI Appendix*.

Preparation of β_2AR Modulators. Compounds were purchased from Chembridge (San Diego, CA). The compounds were procured at 5–25 mmol quantity and dissolved in 10% DMSO to prepare 10 mM stock solutions.

Cell Culture. *HEK293 cells*: HEK293 cell lines were obtained from the American Type Culture Collection (ATCC) and maintained in Dulbecco's modified Eagle's medium (DMEM) as described previously (41).

Human ASM cells: Human ASM cells were isolated from deidentified donor lungs and cultured using F-12 media supplemented with 10% FBS, penicillin and streptomycin, HEPES buffer, $CaCl_2$, L-Glutamine (Gibco, Waltham, MA), and NaOH between 2 and 6 passages as described previously (56). Donor lungs were obtained from National Disease Research Institute and use of cells and tissues from deidentified donors have been judged to be Not Human Subjects research by TJU IRB.

Transfection of HEK293 Cells. *cDNA Constructs and Transfections:* The human β_2AR cDNA containing 3-HA tag at N terminus subcloned into a pcDNA3.1 was obtained from www.cdna.org. Binding site residues PHE(F)282, TYR(Y)219, and ARG(R)131 were mutated to different amino acids using the QuikChange II XL Site-Directed Mutagenesis Kit (Agilent, Santa Clara, CA) per the manufacturer's protocol. Mutations were confirmed by DNA sequencing. HEK293 cells were transfected with cDNA expressing (wild type or mutant; see below) human β_2AR using Lipofectamine 3000 (Invitrogen, Waltham, MA) and used for studies within 36–48 h, or were maintained in media containing G418 at 500 μg/ml concentration. Expression of β_2AR was confirmed by western blotting and confocal imaging using an anti-HA antibody (41).

cAMP Assay. Cells were grown to full confluency in 24-well plates, serum-starved for 24 h, and then incubated with 1 mM IBMX for 10 min. Cells were then incubated with ISO (1 nM to 10 μM) or β_2AR modulators alone or concomitantly for 10 min and cAMP levels were measured by ELISA (Life Technologies, Waltham, MA) as described previously (57, 58).

Arrestin Recruitment to the β_2AR Assay (Bioluminescence Resonance Energy Transfer; BRET). β-agonist-induced recruitment of β-arrestin to the β_2AR was assessed by BRET assay as described previously (40). HEK293 cells were transfected with pcDNA-β-arrestin2-GFP10 and pcDNA3-β_2AR-RlucII, and after 48 h the cells were treated with increasing concentration of ISO and vehicle or 100 nM PAMs or NAMs followed by the addition of Coelenterazine 400a for 20 min. Change in BRET was measured using a Tecan Infinite F500 microplate reader. BRET ratios were calculated by dividing the intensity of light emitted by the GFP10 acceptor by the total light emitted by the RLucII donor.

Radioligand Binding Assay. Competitive radioligand binding assay was performed as previously described (59). Cells expressing β_2AR were lysed and cell membranes were incubated in 3 nM [^{3}H]-dihydroalprenolol ([^{3}H]DHA) with increasing concentration of ISO ± AMs. Bound radioactivity was measured with a TriCarb 4910 TR liquid scintillation analyzer (PerkinElmer, Waltham, MA) and expressed as % of maximum [^{3}H]DHA specific binding. Nonspecific binding was assessed with 10 μM alprenolol. Binding competition curves were generated using nonlinear regression curve fitting function log(inhibitor) vs. response (three parameter) in GraphPad Prism and normalized to percentage of maximal [^{3}H] DHA specific binding.

Immunoassays. Cells were lysed in RIPA buffer (Cell Signaling Technology, Denvers, MA) containing protease and phosphatase inhibitors (Bimake, Houston, TX) after treating with agonists for 10 min. Proteins were separated using SDS-PAGE, transferred onto nitrocellulose membranes, and probed with primary antibodies phospho-ERK1/2 and β-actin. Secondary antibody (Li-Cor) was used to quantify target protein using Odyssey scanner (Li-Cor, Lincoln, NE) and analyzed using ImageStudio software (Li-Cor, Lincoln, NE) as described previously (41, 60).

Receptor Internalization. ISO induced receptor internalization was assessed via cell surface ELISA as previously described (41, 60). Briefly, HEK-293 cells expressing β_2AR were plated on 24-well plates. Cells were treated with100 nM ISO with vehicle or 100 nM AMs for 15 min. Post treatment, cells were washed and fixed with 10% formalin-buffered saline for 10 min on ice, washed twice, and further processed using horseradish peroxidase-conjugated chicken polyclonal anti-HA antibody (Abcam). Cells were washed and incubated with 3,3′,5,5′-tetramethylbenzidine substrate and transferred to a 96-well plate containing sulfuric acid to stop the colorimetric reaction. FlexStation3 was used to measure absorbance at 450 nm. All values were normalized to basal value (no ISO/AMs) of wild-type receptor.

ASM Cell Contraction Using Collagen Gel. Onto a 96-well plate, 100 μl ASM cell suspension (5×10^5 cells/ml) containing type-I rat tail collagen (1.5 mg/ml) in F-12 medium was seeded (61). After 24 h, collagen gels were loosened from the plate. The contraction was initiated by adding histamine (10 μM), with or without

pretreatment with increasing concentration of ISO, with vehicle or AMs for 10 min prior to histamine. Images were obtained using an EVOS live tissue microscope before and at 10-min intervals for 40 min after the addition of histamine. Gel area was obtained for each of the mages using NIH ImageJ software. Data were expressed as percentage gel contraction and calculated using the following equation: [(T0 gel area - T10 gel area) / T0 gel area × 100%].

Ex Vivo Airway Functional Studies Using Murine Precision-Cut Lung Slices. FVB mice expressing human β_2AR in smooth muscle were used in this study (62). The protocol for animal experiments is approved by the Institutional Animal Care and Use Committee at Thomas Jefferson University. Murine lungs were perfused with 4% low-melting agarose, allowed to solidify at 4 for 1 h. For human airways, a small lobe was inflated with 2% low melting point agarose and cores of 8 mm in diameter were made. Both human and murine lungs were then sliced (~250 μm thick) using an oscillating tissue slicer (OTS-5000, FHC Inc). Lung slices cultured for 48 h were treated with methacholine (MCh, 1 μM), and images of the airways were obtained before and 10 min after MCh stimulation using EVOS FL Auto (Life technologies, Waltham, MA) microscope (63). The lung slices were treated with ISO (1 nM – 10 μ M) with vehicle or AMs, and images of the airways were captured at 10-min intervals for a total of 50 min. Images of airways were used to calculate the area of airways using Image J software (NIH). Data from lung slice experiments were plotted as a percentage of methacholine-induced decrease in airway area compared with baseline area.

Statistical Analysis. All data are presented as mean ± Standard Error of Means (SEM) values from '*n*' number of lines derived from different donors in the case of human ASM cells and human and murine tissues. For experiments with HEK293 cells, *'n'* represents technical replicates. Densitometry data from western blot analyses are normalized using band intensities in vehicle-treated cells. cAMP concentrations were determined by extrapolation from a standard curve. One/Two-way ANOVA with Bonferroni post hoc analysis or Student's *t* test was used to determine statistical differences among treatment groups using GraphPad Prism VI software (La Jolla, CA) as described in figure legends. A $P \leq 0.05$ was considered sufficient to reject the null hypothesis.

Data, Materials, and Software Availability. All study data are included in the article and/or *SI Appendix*.

ACKNOWLEDGMENTS. This work is funded by the NIH grants AI135082 (to D.A.D. and A.D.M), HL137030, HL146645 (to D.A.D.), AI161296, AI110007 (to R.B.P.) and GM131710 (to A.D.M.) the Computer-Aided Drug Design Center at the University of Maryland Baltimore for computing time.

Author affiliations: [a]Center for Translational Medicine, Jane and Leonard Korman Respiratory Institute, Philadelphia, PA 19107; [b]Department of Pharmaceutical Sciences, School of Pharmacy, University of Maryland Computer-Aided Drug Design Center, University of Maryland, Baltimore, MD 21201; and [c]Department of Biochemistry and Molecular Biology, Thomas Jefferson University, Philadelphia, PA 19107

1. D. A. Deshpande, R. B. Penn, Targeting G protein-coupled receptor signaling in asthma. *Cell. Signal.* **18**, 2105–2120 (2006).
2. S. R. Salpeter, An update on the safety of long-acting beta-agonists in asthma patients using inhaled corticosteroids. *Expert Opin. Drug Saf.* **9**, 407–419 (2010).
3. S. R. Salpeter, N. S. Buckley, T. M. Ormiston, E. E. Salpeter, Meta-analysis: Effect of long-acting beta-agonists on severe asthma exacerbations and asthma-related deaths. *Ann. Intern. Med.* **144**, 904–912 (2006).
4. W. O. Spitzer *et al.*, The use of beta-agonists and the risk of death and near death from asthma. *N. Engl. J. Med.* **326**, 501–506 (1992).
5. D. R. Taylor, The beta-agonist saga and its clinical relevance: On and on it goes. *Am. J. Respir. Crit. Care Med.* **179**, 976–978 (2009).
6. H. S. Nelson *et al.*, The salmeterol multicenter asthma research trial: A comparison of usual pharmacotherapy for asthma or usual pharmacotherapy plus salmeterol. *Chest* **129**, 15–26 (2006).
7. J. K. Walker, R. B. Penn, N. A. Hanania, B. F. Dickey, R. A. Bond, New perspectives regarding beta(2)-adrenoceptor ligands in the treatment of asthma. *Br. J. Pharmacol.* **163**, 18–28 (2011).
8. R. B. Penn, R. A. Bond, J. K. Walker, GPCRs and arrestins in airways: Implications for asthma. *Handb. Exp. Pharmacol.* **219**, 387–403 (2014).
9. D. A. Deshpande, B. S. Theriot, R. B. Penn, J. K. Walker, Beta-arrestins specifically constrain beta2-adrenergic receptor signaling and function in airway smooth muscle. *FASEB J.* **22**, 2134–2141 (2008).
10. D. A. Deshpande *et al.*, Exploiting functional domains of GRK2/3 to alter the competitive balance of pro- and anticontractile signaling in airway smooth muscle. *FASEB J.* **28**, 956–965 (2014).
11. L. P. Nguyen *et al.*, Beta2-adrenoceptor signaling in airway epithelial cells promotes eosinophilic inflammation, mucous metaplasia, and airway contractility. *Proc. Natl. Acad. Sci. U.S.A.* **114**, E9163–E9171 (2017).
12. T. Pera *et al.*, Specificity of arrestin subtypes in regulating airway smooth muscle G protein-coupled receptor signaling and function. *FASEB J.* **29**, 4227–4235 (2015).
13. N. Al-Sawalha *et al.*, Epinephrine activation of the beta2-adrenoceptor is required for IL-13-induced mucin production in human bronchial epithelial cells. *PLoS One* **10**, e0132559 (2015).
14. N. A. Hanania *et al.*, Response to salbutamol in patients with mild asthma treated with nadolol. *Eur. Respir. J.* **36**, 963–965 (2010).
15. R. Joshi *et al.*, Effects of beta-blockers on house dust mite-driven murine models pre- and post-development of an asthma phenotype. *Pulm. Pharmacol. Ther.* **46**, 30–40 (2017).
16. J. M. Knight *et al.*, Long-acting beta agonists enhance allergic airway disease. *PLoS One* **10**, e0142212 (2015).
17. V. J. Thanawala *et al.*, Beta2-adrenoceptor agonists are required for development of the asthma phenotype in a murine model. *Am. J. Respir. Cell Mol. Biol.* **48**, 220–229 (2013).
18. V. J. Thanawala *et al.*, Beta-blockers have differential effects on the murine asthma phenotype. *Br. J. Pharmacol.* **172**, 4833–4846 (2015).
19. A. Bock, M. Bermudez, Allosteric coupling and biased agonism in G protein-coupled receptors. *FEBS J.* **288**, 2513–2528 (2021).
20. P. J. Conn, A. Christopoulos, C. W. Lindsley, Allosteric modulators of GPCRs: A novel approach for the treatment of CNS disorders. *Nat. Rev. Drug Discov.* **8**, 41–54 (2009).
21. X. Liu *et al.*, Mechanism of intracellular allosteric beta2AR antagonist revealed by X-ray crystal structure. *Nature* **548**, 480–484 (2017).
22. X. Liu *et al.*, An allosteric modulator binds to a conformational hub in the beta2 adrenergic receptor. *Nat. Chem. Biol.* **16**, 749–755 (2020).
23. X. Liu *et al.*, Mechanism of beta2AR regulation by an intracellular positive allosteric modulator. *Science* **364**, 1283–1287 (2019).
24. S. Ahn *et al.*, Allosteric "beta-blocker" isolated from a DNA-encoded small molecule library. *Proc. Natl. Acad. Sci. U.S.A.* **114**, 1708–1713 (2017).
25. B. Pani *et al.*, Unique positive cooperativity between the beta-arrestin-biased beta-blocker carvedilol and a small molecule positive allosteric modulator of the beta2-adrenergic receptor. *Mol. Pharmacol.* **100**, 513–525 (2021).
26. J. Wang *et al.*, Beta-arrestin-biased allosteric modulator potentiates carvedilol-stimulated beta adrenergic receptor cardioprotection. *Mol. Pharmacol.* **100**, 568–579 (2021).
27. O. Guvench, A. D. MacKerell Jr., Computational fragment-based binding site identification by ligand competitive saturation. *PLoS Comput. Biol.* **5**, e1000435 (2009).
28. E. P. Raman, W. Yu, S. K. Lakkaraju, A. D. Mackerell Jr., Inclusion of multiple fragment types in the site identification by ligand competitive saturation (SILCS) approach. *J. Chem. Inf. Model.* **53**, 3384–3398 (2013).
29. D. R. Weiss, M. Levitt, Can morphing methods predict intermediate structures? *J. Mol. Biol.* **385**, 665–674 (2009).
30. A. D. MacKerell Jr., S. Jo, S. K. Lakkaraju, C. Lind, W. Yu, Identification and characterization of fragment binding sites for allosteric ligand design using the site identification by ligand competitive saturation hotspots approach (SILCS-Hotspots). *Biochim. Biophys. Acta Gen. Subj.* **1864**, 129519 (2020).
31. G. A. Heinzl *et al.*, Iminoguanidines as allosteric inhibitors of the iron-regulated heme oxygenase (HemO) of pseudomonas aeruginosa. *J. Med. Chem.* **59**, 6929–6942 (2016).
32. A. Gomes *et al.*, Insights into glucose-6-phosphate allosteric activation of beta-Glucosidase A. *J. Chem. Inf. Model.* **61**, 1931–1941 (2021).
33. W. Yu, S. K. Lakkaraju, E. P. Raman, L. Fang, A. D. MacKerell Jr., Pharmacophore modeling using site-identification by ligand competitive saturation (SILCS) with multiple probe molecules. *J. Chem. Inf. Model.* **55**, 407–420 (2015).
34. E. P. Raman, W. Yu, O. Guvench, A. D. Mackerell, Reproducing crystal binding modes of ligand functional groups using site-identification by ligand competitive saturation (SILCS) simulations. *J. Chem. Inf. Model.* **51**, 877–896 (2011).
35. S. K. Lakkaraju *et al.*, Mapping functional group free energy patterns at protein occluded sites: Nuclear receptors and G-protein coupled receptors. *J. Chem. Inf. Model.* **55**, 700–708 (2015).
36. S. K. Lakkaraju, E. P. Raman, W. Yu, A. D. MacKerell Jr., Sampling of organic solutes in aqueous and heterogeneous environments using oscillating μex grand canonical-like monte carlo-molecular dynamics simulations. *J. Chem. Theory Comput.* **10**, 2281–2290 (2014).
37. D. R. Koes, C. J. Camacho, Pharmer: Efficient and exact pharmacophore search. *J. Chem. Inf. Model.* **51**, 1307–1314 (2011).
38. T. Oashi, A. L. Ringer, E. P. Raman, A. D. Mackerell, Automated selection of compounds with physicochemical properties to maximize bioavailability and druglikeness. *J. Chem. Inf. Model.* **51**, 148–158 (2011).
39. S. J. Horvat *et al.*, A-kinase anchoring proteins regulate compartmentalized cAMP signaling in airway smooth muscle. *FASEB J.* **26**, 3670–3679 (2012).
40. J. Quoyer *et al.*, Pepducin targeting the C-X-C chemokine receptor type 4 acts as a biased agonist favoring activation of the inhibitory G protein. *Proc. Natl. Acad. Sci. U.S.A.* **110**, E5088–E5097 (2013).
41. S. Naik *et al.*, Regulation of cysteinyl leukotriene type 1 receptor internalization and signaling. *J. Biol. Chem.* **280**, 8722–8732 (2005).
42. T. G. Zaremba, P. H. Fishman, Desensitization of catecholamine-stimulated adenylate cyclase and down-regulation of beta-adrenergic receptors in rat glioma C6 cells. Role of cyclic AMP and protein synthesis. *Mol. Pharmacol.* **26**, 206–213 (1984).
43. S. J. Morgan *et al.*, Beta-agonist-mediated relaxation of airway smooth muscle is protein kinase A-dependent. *J. Biol. Chem.* **289**, 23065–23074 (2014).
44. H. Goel, A. Hazel, W. Yu, S. Jo, A. D. MacKerell Jr., Application of site-identification by Ligand competitive saturation in computer-aided drug design. *New J. Chem.* **46**, 919–932 (2022).
45. R. C. Bernardi, M. C. R. Melo, K. Schulten, Enhanced sampling techniques in molecular dynamics simulations of biological systems. *Biochim. Biophys. Acta* **1850**, 872–877 (2015).
46. A. M. Schonegge *et al.*, Evolutionary action and structural basis of the allosteric switch controlling beta2AR functional selectivity. *Nat. Commun.* **8**, 2169 (2017).
47. S. G. Rasmussen *et al.*, Crystal structure of the beta2 adrenergic receptor-Gs protein complex. *Nature* **477**, 549–555 (2011).
48. S. Chen *et al.*, Mutation of a single TMVI residue, Phe(282), in the beta(2)-adrenergic receptor results in structurally distinct activated receptor conformations. *Biochemistry* **41**, 6045–6053 (2002).

49. R. U. Malik *et al.*, Detection of G protein-selective G protein-coupled receptor (GPCR) conformations in live cells. *J. Biol. Chem.* **288**, 17167–17178 (2013).
50. M. Choi *et al.*, G protein-coupled receptor kinases (GRKs) orchestrate biased agonism at the beta2-adrenergic receptor. *Sci. Signal.* **11**, eaar7084 (2018).
51. R. J. Lefkowitz, K. L. Pierce, L. M. Luttrell, Dancing with different partners: Protein kinase a phosphorylation of seven membrane-spanning receptors regulates their G protein-coupling specificity. *Mol. Pharmacol.* **62**, 971–974 (2002).
52. S. R. Salpeter, N. S. Buckley, Systematic review of clinical outcomes in chronic obstructive pulmonary disease: Beta-agonist use compared with anticholinergics and inhaled corticosteroids. *Clin. Rev. Allergy Immunol.* **31**, 219–230 (2006).
53. S. R. Salpeter, A. J. Wall, N. S. Buckley, Long-acting beta-agonists with and without inhaled corticosteroids and catastrophic asthma events. *Am. J. Med.* **123**, 322–328.e322 (2010).
54. G. S. Forkuo *et al.*, Phosphodiesterase 4 inhibitors attenuate the asthma phenotype produced by beta2-adrenoceptor agonists in phenylethanolamine n-methyltransferase-knockout mice. *Am. J. Respir. Cell Mol. Biol.* **55**, 234–242 (2016).
55. F. J. Nunez *et al.*, Agonist-specific desensitization of PGE2-stimulated cAMP signaling due to upregulated phosphodiesterase expression in human lung fibroblasts. *Naunyn Schmiedebergs Arch. Pharmacol.* **393**, 843–856 (2020).
56. R. A. Panettieri, R. K. Murray, L. R. DePalo, P. A. Yadvish, M. I. Kotlikoff, A human airway smooth muscle cell line that retains physiological responsiveness. *Am. J. Physiol.* **256**, C329–C335 (1989).
57. J. V. Michael *et al.*, Cooperativity of E-prostanoid receptor subtypes in regulating signaling and growth inhibition in human airway smooth muscle. *FASEB J.* **33**, 4780–4789 (2019).
58. S. K. Yadav *et al.*, Autocrine regulation of airway smooth muscle contraction by diacylglycerol kinase. *J. Cell Physiol.* **237**, 603–616 (2021), 10.1002/jcp.30528.
59. F. De Pascali *et al.*, Beta2 -adrenoceptor agonist profiling reveals biased signalling phenotypes for the beta2 -adrenoceptor with possible implications for the treatment of asthma. *Br. J. Pharmacol.* **179**, 4692–4708 (2022), 10.1111/bph.15900.
60. A. P. Nayak *et al.*, Regulation of ovarian cancer G protein-coupled receptor-1 expression and signaling. *Am. J. Physiol. Lung Cell. Mol. Physiol.* **316**, L894–L902 (2019).
61. T. J. Harford *et al.*, Respiratory syncytial virus induces beta2-adrenergic receptor dysfunction in human airway smooth muscle cells. *Sci. Signal.* **14**, eabc1983 (2021).
62. D. W. McGraw *et al.*, Transgenic overexpression of beta(2)-adrenergic receptors in airway smooth muscle alters myocyte function and ablates bronchial hyperreactivity. *J. Biol. Chem.* **274**, 32241–32247 (1999).
63. A. Bergner, M. J. Sanderson, Airway contractility and smooth muscle Ca(2+) signaling in lung slices from different mouse strains. *J. Appl. Physiol. (1985)* **95**, 1325–1332; discussion 1314 (2003).